Feedstock-Dependent Nitrogen Configurations of Nitrogen-Doped Single-Walled Carbon Nanotubes in CVD Process

Theerapol Thurakitseree,*[a] Christian Kramberger,[b] and Shigeo Maruyama*[c,d]

Received Xth XXXXXXXXXX 20XX, Accepted Xth XXXXXXXXX 20XX
First published on the web Xth XXXXXXXXXX 200X
DOI: 10.1039/b000000x

The modification of nitrogen configuration is a viable way to control the electronic properties of nitrogen-doped single-walled carbon nanotube (N-doped SWCNT). N-doped SWCNTs were synthesized by a conventional chemical vapor deposition process with mixed carbon/nitrogen (C/N) feedstock. While higher feedstock flow rates promote the formation of encapsulated N_2 molecules, lower flow rates show a predominance of pyridinic and graphitic nitrogen structures as revealed by X-ray photoemission spectroscopy. Therefore the nitrogen doping in the sp^2 carbon network can be controlled by the flow rate of the C/N feedstock.

1 Introduction

The properties of single-walled carbon nanotubes (SWCNT) can be modified by incorporating dopants into the sp^2 carbon network[1–4]. To that aim Nitrogen (N) is a very interesting dopant[3–6], which can either provide *p*- or *n*-types doping, merely depending on how it arranges itself to bond with the surrounding sp^2 carbon. Additionally, it can also affect catalyst particles while growing nanotubes and lead to a reduction of nanotube diameters[6–8]. In general the electronic properties of N-doped SWCNTs can be affected by three different configurations of N incorporation into the sp^2 carbon structure[9]. One principal configuration is to substitute one C directly with one N. In this case, one free electron is forced to occupy the localized π^* state, rendering substitutional N an electron donor (*n*-type). The other two pyridinic N configurations exhibit electron acceptor behavior due to localized π electrons and consequently *p*-type doping.

These different N configurations are commonly observed in N-doped SWCNTs obtained in well-established synthesis processes[4–6]. The relative yield of the different species of incorporated N was shown to be controlled by changing growth temperature[5] or feedstock concentration[6,7], yet the influence of precursor flow rate on the relative yield of different N species has not been reported. P. Ayala *et al.*[5] have previously demonstrated changes in the doping profile of N with the growth temperature, encapsulated N_2 was observed at growth temperature lower than 800°C. Encapsulated N_2 molecules are commonly observed in multi-walled carbon nanotubes[10,11] but can also exist in N-doped SWCNTs. In our previous report[12], we have demonstrated the existance of one-dimensional chains of encapsulated N_2 molecules inside small-diameter N-doped SWCNTs. Changes in the N doping profile were also observed by changing the additional ammonia feed[6] atop a constant feed of acetylene.

Here we demonstrate that the N configuration can indeed be modified by changing the C/N feedstock flow rate in activated thermal chemical vapor deposition (CVD) in which the feedstock was continuously purged during the CVD reaction. As compared to no-flow CVD in our previous report[8], diameter control of N-doped SWCNTs seems to be not significantly affected by the feedstock introduction process even at low feedstock flow rate. However, the N1s core level spectra as measured by X-ray photoemission reveals a clear effect of low flow rates on the frequencies of the distinct N configurations. At low feedstock flow rates, the yield of encapsulated molecular N_2 declines as N incorporation into the sp^2 C network becomes predominant within the on overall significantly increased amount of incorporated N.

2 Materials & Methods

N-doped SWCNTs were synthesized by conventional CVD[13–15]. A 20% acetonitrile mixture in ethanol was used as mixed C/N feedstock. The bimetallic Co/Mo catalyst particles for the nanotube growth were prepared by liquid-dip coating of silicon substrates. The ethanol solution contained 0.1 wt.% each of cobalt (Co) and molybdenum (Mo) acetate[16].

Prior to the CVD reaction, the Co/Mo catalyst was reduced

[a] *Program in Applied Physics, Maejo University, Chiang Mai, 50290 Thailand. Fax: 66 53 878225; Tel: 66 53 873515; E-mail: theerapol@mju.ac.th*
[b] *Faculty of Physics, Technische Universität Wien, Vienna, 1040 Austria.*
[c] *Department of Mechanical Engineering, University of Tokyo, Tokyo, 113-8656 Japan.*
[d] *National Institute of Advanced Industrial Science and Technology, Tsukuba, 305-8564 Japan. Fax: 81 3 5800 6983; Tel: 81 3 5841 6421; E-mail: maruyama@photon.t.u-tokyo.ac.jp*

under 3% H_2 in Ar atmosphere. When the fixed growth temperature of 800°C was reached, the reducing gas was evacuated to the background pressure of 14 Pa. The feedstock mixture was then released into CVD chamber. While the downstream part of the reactor was kept evacuating, the feedstock flow rate was varied from 20 to 450 sccm. The reaction was run for 10 min at a pressure of 1.3 kPa before the atmosphere was replaced by Ar, and the CVD setup was cooled down to room temperature.

As-grown SWCNT films were transferred onto Si wafer[17] and heated to dehydrate the samples. The transferred films were characterized by resonance Raman spectroscopy (Jobin Yvon Horiba with T64000 triple monochromator) at an excitation wavelength of 532 nm. The local chemical shifts of carbon and nitrogen were analyzed by photoelectron spectroscopy (XPS) measured with a PHI 5000 VersaProbe setup at $AlK_\alpha = 1.486$ keV (the beam size of 100 μm in diameter) on the transferred samples. The additional Mo 3d spectra were also measured on the samples synthesized from low-flow rate of C/N feedstocks. A thin layer of Au was sputtered on top of as-grown samples for morphology observation by scanning electron microscopy (SEM, JSM-6335F, Jeol Ltd.). For additional morphology observation of N-doped SWCNTs synthesized from low-flow rate of C/N feedstocks (20 and 100 sccm), as-grown N-doped SWCNTs on Si were dispersed in ethanol (see Supporting information). Dispersed nanotubes were observed by transmission electron microscopy (TEM, JEOL JEM-2010 operated at 200 kV).

For heterojunction diode fabrication of N-doped SWCNTs, the as-grown nanotubes synthesized from 20 sccm were transferred onto *p*-type Si substrate without oxide layer. The Au layer with the thickness of 40 nm was then deposited on the film as depicted in the inset of Fig. 7. The aluminium paste was used as anode electrode. The current-voltage (*I-V*) measurement was performed in ambient condition.

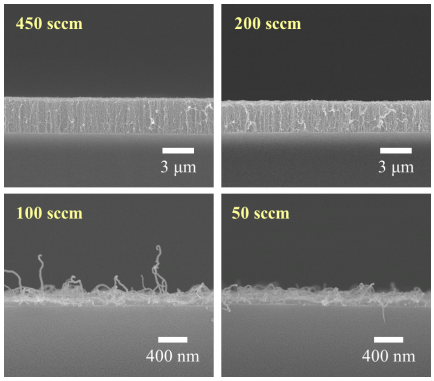

Fig. 1 SEM micrographs of N-doped SWCNT films synthesized from different flow rates of C/N feedstock.

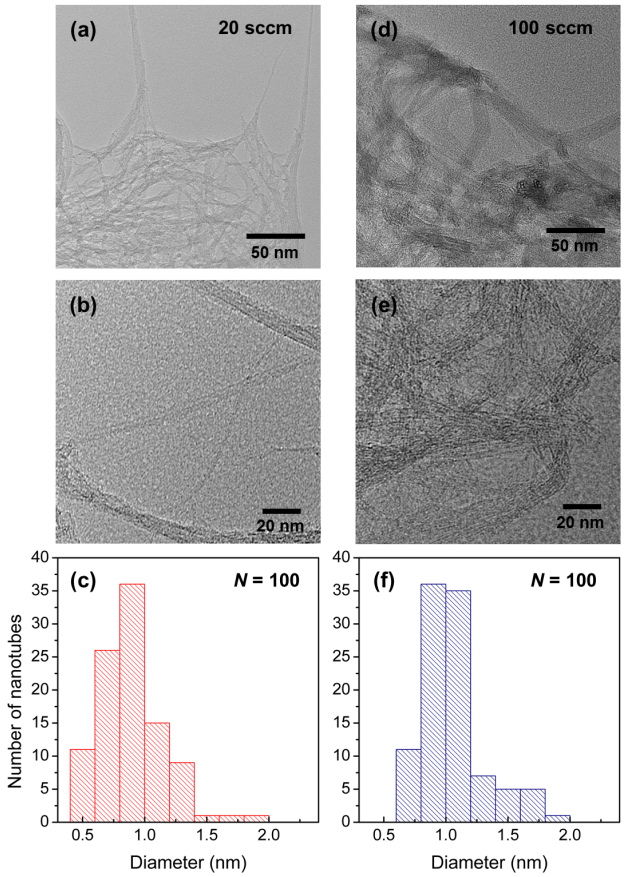

Fig. 2 TEM images and of N-doped SWCNTs synthesized from flow rate of 20 sccm (a,b) and 100 sccm (d,e) of C/N feedstocks, and histograms showing SWNT diameter distributions obtained from TEM observations of N-doped SWCNTs synthesized from flow rate of 20 sccm (c) and 100 sccm (f). The observed mean diameters are 0.89±0.25 nm and 1.06±0.24 nm, respectively.

3 Results & Discussion

Fig. 1 shows SEM micrographs of as-grown N-doped SWCNT films synthesized from 20% of acetonitrile mixture in ethanol with different feedstock flow rates varied from 20 sccm to 450 sccm. Vertically aligned growth could be observed at high feedstock flow rates (more than 200 sccm), while the thickness of nanotube forests quickly decreased with lower flow rate. Note that SEM observation under high magnification with the influence of charging effect and deposition of gold nanoparticles during sample preparation could make the nanotubes feature becomes larger, which can be typically observed when the nanotube density is low[18]. To clarify the nanotube morphology in case of lower-flow rate, the additional TEM observation was performed as seen in Fig. 2. It can cleary seen that even though flow rate of the C/N feedstock was reduced during the

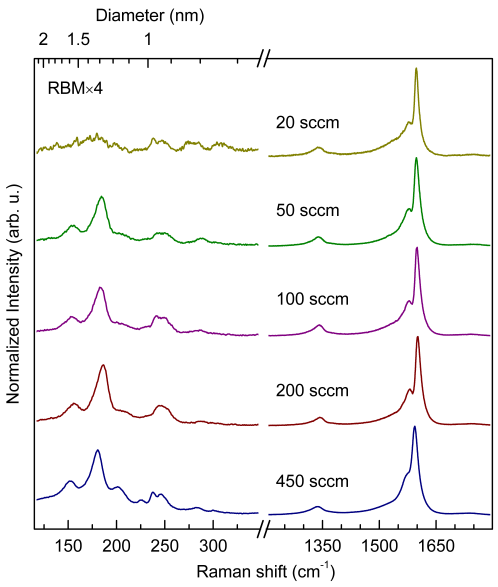

Fig. 3 Raman spectra recorded at 532 nm excitation wavelength show a relative increase in small-diameter RBM peaks and more pronounced G-line splitting with decreasing feedstock flow rates.

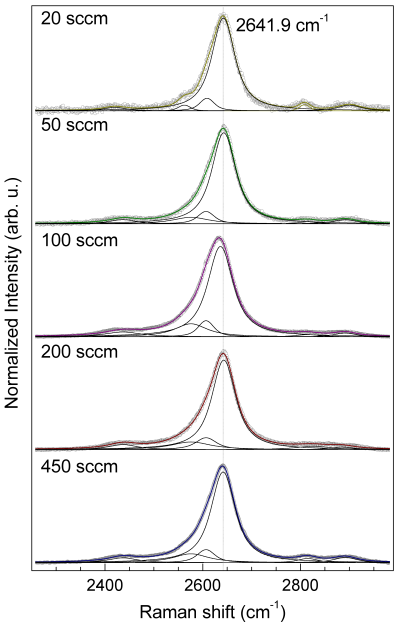

Fig. 4 Raman spectra of the 2D-band of N-doped SWCNT films obtained at an excitation wavelength of 532 nm.

reaction, the nanotube morphology is still retained to be single wall for both 20 sccm (Fig. 2a,b) and 100 sccm (Fig. 2d,e). However, at flow rates of 200 sccm and above the thickness of the SWCNT films is rather uniform as the growth is well saturated within 10 min.

Fig. 3 shows resonance Raman spectra of as-grown N-doped SWCNT films obtained with an excitation wavelength of 532 nm. The tangential G-band feature from atomic vibration along the axial direction do not show significant changes with feedstock flow rate. The uniform sharp D-band indicates a constant quality in all samples of N-doped-SWCNTs. Nanotube diameters are accessible via the radial breathing mode (RBM), of the SWCNTs that are in resonance with an excitation wavelength of 532 nm. It has been shown that the well resolved RBM peaks at 145 and 180 cm^{-1} are characteristic features of vertical aligned growth[19]. These peaks are clearly more pronounced for N-doped SWCNT films synthesized with high flow rates above 200 sccm, whereas the reduced intensity at lower flow rates is attributed to the ever lesser relative contribution of upright SWCNTs due to less bundling of random nanotubes, indicating that the nanotube population and their morphology play an active role on the RBM intensity. We evaluated nanotube diameters following the empirical relation[20]. According to the Kataura plot[20], the resonance of the observed RBM peaks stem from the first metallic transition (E_{11}^{M}).

With decreasing flow rates the high frequency RBM peaks at 280 and 300 cm^{-1} from the smallest diameters become relatively stronger, as the lower frequency RBM peaks are reduced in intensity which is in consistent with the diameter distributions of N-doped SWCNTs synthesized from 20 and 100 sccm observed from TEM observation (Fig. 2c,f). The gradual promotion of smaller diameters in the distribution leaves also a clear signature in the G-band which shows a more pronounced splitting of the G^- and the G^+ components.

Fig. 4 compares the Raman spectra of the 2D-band (or G′) in N-doped SWCNTs synthesized at the different feedstock flow rates. The G′ lines were decomposed and fitted with Voigtian peaks with a constant full-width at half maximum (FWHM) of 13.6 cm^{-1}. The primary peak at 2641.6 cm^{-1} is observed in all cases. At the lowest flow rate of 20 sccm the 2D band shows weak additional components at 2560 and 2800 cm^{-1} which can not be assigned to the second order overtone of SWCNTs, they are rather indicative of high curvature graphitic shell particle[21] and defective sites of graphitic sp^2 C network[22], respectively. Such carboneous species may be anticipated to form on inactive catalyst particles residing at the surface of the silicon substrate. From our previous report[23], the main peak obtained from the samples synthesized by continuous flow CVD condition seems to be different from that obtained from 5% acetonitrile feedstock mixture in ethanol in no-flow CVD. The peak feature, on the other hand, has similar shape to the G′ line of SWCNT film synthesized from pure ethanol. Even though 20% acetonitrile was mixed into ethanol feedstock, this suggests that there was only partial decomposition of the mixed precursors during CVD reaction. Then

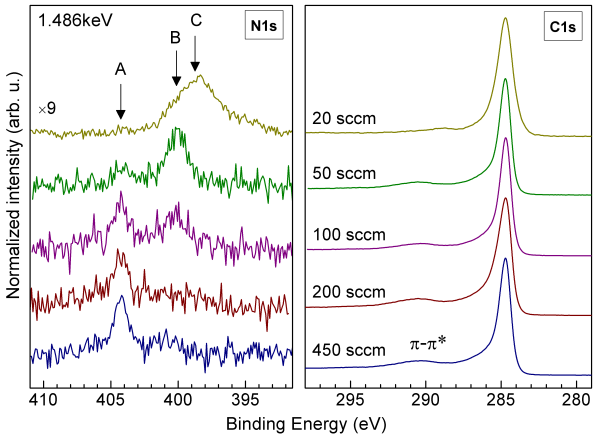

Fig. 5 XPS spectra of N-doped SWCNTs reveal a shift from trapped N_2 molecules to incorporated N with decreasing flow rate.

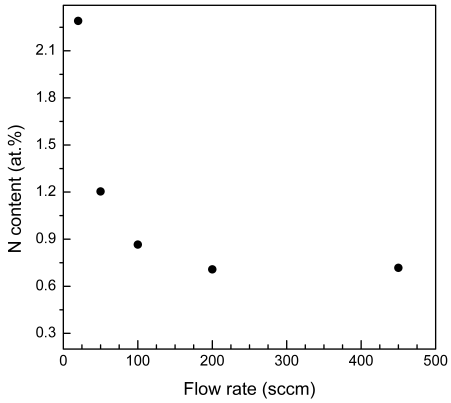

Fig. 6 Total nitrogen concentration as function of C/N feedstock flow rate during the growth.

the nitrogen could not play an efficient active role to reduce the nanotube diameter as seen in weak small-diameter RBM peaks (Fig. 3) and a slight difference in the nanotube mean diameter in case of 20 and 100 sccm flow rates (Fig. 2c,f).

The bonding environment of nitrogen in the sp^2 carbon network was characterized by XPS spectroscopy (Fig 5). After dehydrating the SWCNT films, only neglibile oxygen content was observed for all samples (not shown here). The only two main peaks were represented in the range of 279 eV to 298 eV and 391 eV to 411 eV for carbon and nitrogen, respectively. Fig. 5 shows a common narrow asymmetric Doniach Šunjić lineshape in the sp^2 C1s of N-doped SWCNTs synthesized with different feedstock flow rates. The binding energy of the C1s was found to be at 284.6 eV as seen in previous reports with $\pi - \pi^*$ electron shake up[5,7,24]. Note that there is no shift in C1s peak position with changing C/N feedstock flow rates. However strongly varying chemical profiles of nitrogen are observed for different flow rates. From Fig 5, the binding energy of about 404 eV indicates the presence of encapsulated N_2 molecules inside the nanotubes[10,12], while signals from both substitutional and pyridinic N configurations are anticipated in the range of 398–400 eV[5,7,12]. At higher flow rates where thick SWCNT films are formed there is an evident predominance of trapped N_2 molecules, whereas there is a clear dominance of substitutional and pyridinic N incorporation in thin N doped SWCNT films. This difference shows that the growth dynamics are crucial for the achievable N doping. At a high throughput of radical CN species in the catalyst particle, more N_2 is formed before the CN units could be possibly incorporated into the participating sp^2 C walls. On the other hand, less N_2 molecules are formed with more incorporated N into sp^2 C structure as C/N feedstock flow rate decreased. At low flow rates, the strong CN bonds in diluted precursors could be favoring pathways to pyridinic and substitutional nitrogen incorporation, while the formation of N_2 gas is suppressed. At higher flow rates and consequently higher concentrations of CN species in the catalyst particles, an increasing fraction of N_2 molecules may be formed instead of the incorporation of nitrogen. This dynamic idea can account for the observed effect of the flow rate on the chemical profile of the nitrogen.

To evaluate N content in N-doped SWCNTs, the 1.8 times higher atomic cross section for N as compared to C and the relative XPS peak intensities were used[25]. The abundance of substitutional and pyridinic nitrogen in N-doped SWCNTs was evaluated as shown in Fig. 6. Fig. 6 shows the nitrogen amount determined from the N1s area. It can be clearly seen that the relative amount of nitrogen is inversely proportional to the feedstock flow rate. It is dramatically increased to approximately three times when the C/N feedstock flow rate is reduced from 100 to 20 sccm. In addition, all the N1s peaks were decomposed using two Voigtian peaks at 400.9 and 404.2 eV in case of 200 and 450 sccm, two Voigtian peaks at 400 and 404.2 eV in case of 50 and 100 sccm, and three Voigtian peaks at 398.2, 400.9 and 404.2 eV for 20 sccm condition to evaluate each N configuration (see Fig. S1). Each nitrogen configuration content was obtained from the decomposed N1s core level. Considering signal-to-noise ratio, the content of each configuration was evaluated compared to the total nitrogen amount using peak areas. As shown in Fig. S2, the amount of N_2 species is drastically reduced to less than 50 % of the total nitrogen content when the feedstock flow rate was lowered from 100 to 20 sccm. On the other hand, the amount of graphitic and pyridinic nitrogen are predominant at lower-flow rate. It should be noted that there is possibility of Mo signal observed from the thin nanotube samples in case of lower-flow rate at a similar binding energy[26]. In order to obtain only the nanotube signal, we performed the XPS measurement on transferred samples. The survey scans of trans-

ferred nanotube samples synthesized from 20 and 100 sccm of C/N feedstock (see Fig. S3) show a strong C1s peaks and a minor O1s peaks. The absence of the signals from Mo 3d core level as shown in Fig. S4 suggests that Mo particles do not detached from the substrate during nanotube transfer due to strong interaction between Co/Mo catalysts and substrate [27]. This reveals that the obtained binding energy of approximately 398 eV belong to the nanotube samples.

Note that the constant D-band intensity at all flow-rates confirms a uniform defect concentration in all N-doped SWCNTs samples due to incorporation of nitrogen and interaction of encapsulated N_2 with carbon walls [28] (Fig. 4). It is thus remarkable for the invariable quality of N-doped SWCNTs in this case as reported earlier [29,30]. N-doping induced defects is typically found in multi-walled carbon nanotubes (MWCNTs) in which nitrogens could incorporated into multigraphitic shells [31–37]. Y. T. Lee *et al.* [37] have demonstrated the effect of growth temperature and ammonia flow rate on production of nitrogen content in MWCNTs. As more ammonia flow rate was added, it was found that the nitrogen content was drastically increased, and diminished when the flow rate was more than 40 sccm. Similarly, using carbon precursor containing different nitrogen sources could also introduce more defects in SWCNTs as feedstock flow rate increases [6,38,39]. F. Villalpando-Paez *et al.* [38] have previously reported N-doped SWCNTs synthesis from thermal decomposition of ferrocene/ethanol/benzylamine solution. Linear increasing of point defects was found to be as a function of nitrogen precursor concentration. A similar tendency was also found when ammonia was used as nitrogen source [6,39]. Y. S. Min *et al.* [39] have reported the use of methane and ammonia as C/N precursor for the synthesis of N-doped SWCNTs. It was found that the D-band to G-band ratio in Raman spectra slightly increases as more nitrogen source was added. H. R. Barzegar *et al.* [6] have demonstrated an increase in N content with increased ammonia feed in which more defect sites were introduced by pyrrolic N during the growth process. It was found that low nitrogen incorporation with a predominance of pyridinic structure was observed at low ammonia feeds. This is in agreement with the appearance of the anticipated XPS peak in the range of 398–400 eV for pyridinic N in our study. A similar binding energy (∼398 eV) of pyridinic N was also found in metal-free grown of N-doped SWCNTs [38]. While the incorporation of N into sp^2 C network can cause a bonding stress to nanotube structure giving rise to high D-band [5,6,24], the constant D line intensity can be considered from saturated N incorporation in nanotubes, interaction between encapsulated N_2 and carbon walls [28], and the rest of N amount has formed graphitic nanoshell as in agreement with the appearance of the 2D line (Fig. 4). This may be the reason why high N incorporation was observed, whereas the imperfection of nanotube structure remained unchanged.

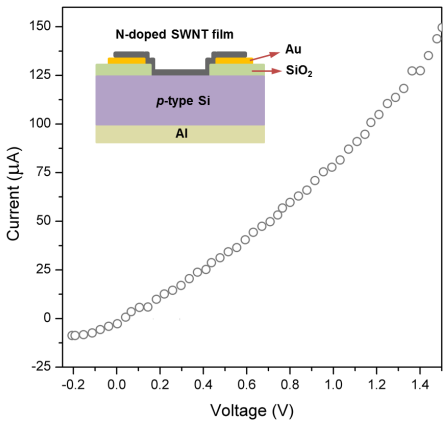

Fig. 7 The *I-V* characteristic of N-doped SWCNTs/*p*-type Si heterojunction deiode in case of 20 sccm C/N feedstock. The schematic of diode is illustrated in the inset.

The total N incorporation in our case, however, shows higher abundunace in N-doped SWCNT samples at low C/N feedstock flow rate, compared to the previous report [8].

Further characteraction of electrical property of N-doped SWCNTs synthesized from 20 sccm of C/N feedstock was performed by heterojunction diode as shown in Fig. 7. The heterojunction diode was fabricated from transferred thin film of N-doped SWCNTs synthesized from 20 sccm of C/N feedstock. The formatin of *p-n* junction leads to *I-V* characteristic of diode turned on at the forward bias direction. This result suggests that the obtained N-doped SWCNTs synthesized from lower flow rate contain more incorporation of sp^2 into the carbon walls.

In our previous report [8], the no-flow CVD was employed to synthesize N-doped SWCNTs from different concentration of acetonitrile-mixture in ethanol. As the feedstock mixture increased, more nitrogen incorporation into the nanotubes was observed and saturated at about 1.2 at.% in which a major configuration of nitrogen was in form of N_2 molecules [12], and the rest was incorporated N into the nanotube walls. The catalyst lifetime was found to be shorter in the presence of more nitrogen incorporation as seen in lower yield of the nanotube film. This may be plausibly due to changing in growth mechanism from tangential to perpendicular growth mode [23] by nitrogen, resulting in smaller in diameter and saturation of carbon precipitation on the catalyst so that the catalyst lifetime could no longer be extended to activate the nanotube formation with more nitrogen incorporation. By considering the the same acetonitrile feedstock mixture concentration (20 %), more nitrogen incorporation could not be proceeded since the feedstock mixture could not leave the system during the CVD reaction in no-flow CVD, resulting in low nitrogen content in the nanotube walls (less than 1 at.%) with abundant of N_2 molecules (∼1 at.%). On the other hand, the decomposition

of C/N feedstock by continuous feedstock supply could produce water molecules spontaneously, which could re-activate the catalyst during the reaction as reported on supergrowth N-doped carbon nanotubes in which acetonitrile was used as nitrogen source[36,40]. Continuous introduction of water during growth could prolong the catalyst lifetime, which allows the nanotubes to keep growing. In our case, this would result in more nitrogen atoms incorporating into the nanotube walls and less N_2 molecules with slow flow rate, but lower nanotube yield due to different growth mechanisms caused nitrogen[23]. However, faster flow-rate of the feedstock leads to inadequate re-activation of the catalyst as seen in low nitrogen content.

4 Conclusions

Upon changing flow rate of carbon/nitrogen feedstock mixture, the nitrogen configuration could be modified during conventional CVD synthesis. The pyridinic and graphitic nitrogen structures are predominant at low flow rate, whereas nitrogen incorporation is more skewed towards to N_2 formation inside the nanotubes. The total nitrogen content at low flow rate was also evaluted to be approximately two to three times higher than that obtained at higher flow rate. The formation of carbon and nitrogen, as evidenced by Raman spectroscopy and diode characteristic, is suggested that graphitic nanoshell particles could be formed along with more defective sp^2 C structure. The ability to alter incorporation of nitrogen into nanotube structure is therefore one important step for modification on SWCNT property.

Acknowledgements

Part of this work was financially supported by the Thailand Research Fund (TRF5780165), and the Official Agricultural Research and Extension, Maejo University; JSPS KAKENHI Grant Numbers JP25107002, JP15H05760, and IRENA Project by JST-EC DG RTD, Strategic International Collaborative Research Program, SICORP. Part of this work is based on results obtained from a project commissioned by the New Energy and Industrial Technology Development Organization (NEDO). We also acknowledge supports from Advanced Characterization Nanotechnology Platform of the University of Tokyo, supported by "Nanotechnology Platform" of the Ministry of Education, Culture, Sports, Science and Technology (MEXT), Japan. CK acknowledges the Austrian Academy of Sciences for the APART fellowship A-11456.

References

1 R. S. Lee, H. J. Kim, J. E. Fischer, A. Thess and R. E. Smalley, *Nature*, 1997, **388**, 255–257.
2 D. Golberg, Y. Bando, W. Han, K. Kurashima and T. Sato, *Chem. Phys. Lett.*, 1999, **308**, 337–342.
3 M. Terrones, P. M. Ajayan, F. Banhart, X. Blase, D. L. Carroll, J. C. Charlier and et al., *Appl. Phys. A*, 2002, **74**, 355–361.
4 D. Yu, Q. Zhang and L. Dai, *J. Am. Chem. Soc.*, 2010, **132**, 15127–15129.
5 P. Ayala, A. Grüneis, T. Gemming, D. Grimm, C. Kramberger, M. H. Rümmeli and et al., *J. Phys. Chem. C*, 2007, **111**, 2879–2884.
6 H. R. Barzegar, E. Gracia-Espino, T. Sharifi, F. Nitze and T. Wągberg, *J. Phys. Chem. C*, 2013, **117**, 25805–25816.
7 E. Ibrahim, V. O. Khavrus, A. Leonhardt, S. Hampel, S. Oswald, M. H. Rümmeli and et al., *Diam. Relat. Mater.*, 2010, **19**, 1199–1206.
8 T. Thurakitseree, C. Kramberger, P. Zhao, S. Aikawa, S. Harish, S. Chiashi and et al., *Carbon*, 2012, **50**, 2635–2640.
9 R. Arenal, K. March, C. P. Ewels, X. Rocquefelte, M. Kociak, A. Loiseau and et al., *Nano Lett.*, 2014, **14**, 5509–5516.
10 A. V. Okotrub, L. G. Bulusheva, A. G. Kudashov, V. V. Belavin, D. V. Vyalikh and S. L. Molodtsov, *Appl. Phys. A*, 2009, **94**, 437–443.
11 L. G. Bulusheva, A. V. Okotrub, Y. V. Fedoseeva, A. G. Kurenya, I. P. Asanov, O. Y. Vilkov and et al., *Phys. Chem. Chem. Phys.*, 2015, **17**, 23741–23747.
12 C. Kramberger, T. Thurakitseree, H. Koh, Y. Izumi, T. Kinoshita, T. Muro and et al., *Carbon*, 2013, **55**, 196–201.
13 S. Maruyama, R. Kojima, Y. Miyauchi, S. Chiashi and M. Kohno, *Chem. Phys. Lett.*, 2002, **360**, 229–234.
14 Y. Murakami, S. Chiashi, Y. Miyauchi, M. Hu, M. Ogura, T. Okubo and et al., *Chem. Phys. Lett.*, 2004, **385**, 298–303.
15 S. Maruyama, E. Einarsson, Y. Murakami and T. Edamura, *Chem. Phys. Lett.*, 2005, **403**, 320–323.
16 Y. Murakami, Y. Miyauchi, S. Chiashi and S. Maruyama, *Chem. Phys. Lett.*, 2003, **377**, 49–54.
17 Y. Murakami and S. Maruyama, *Chem. Phys. Lett.*, 2006, **422**, 575–580.
18 J. Loos, A. Alexeev, N. Grossiord, C. E. Koning and O. Regev, *Ultramicroscopy*, 2005, **104**, 160–167.
19 Y. Murakami, S. Chiashi, E. Einarsson and S. Maruyama, *Phys. Rev. B*, 2005, **71**, 085403.
20 P. T. Araujo, S. K. Doorn, S. Kilina, S. Tretiak, E. Einarsson, S. Maruyama and et al., *Phys. Rev. Lett.*, 2007, **98**, 067401.
21 V. Osipov, A. Baranov, V. Ermakov, T. Makarova, L. Chungong, A. Shames and et al., *Diam. Relat. Mater.*, 2011, **20**, 205–209.
22 A. Eckmann, A. Felten, A. Mishchenko, L. Britnell, R. Krupke, K. S. Novoselov and et al., *Nano Lett.*, 2012, **12**, 3925–3930.
23 T. Thurakitseree, C. Kramberger, A. Kumamoto, S. Chiashi, E. Einarsson and S. Maruyama, *ACS Nano*, 2013, **7**, 2205–2211.
24 S. H. Lim, H. I. Elim, X. Y. Gao, A. T. S. Wee, W. Ji, J. Y. Lee and et al., *Phys. Rev. B*, 2006, **73**, 045402.
25 J. Scofield, *J. Electron Spectrosc. Relat. Phenom.*, 1976, **8**, 129–137.
26 K.-H. Lee, Y.-W. Lee, D.-H. Kwak, J.-S. Moon, A.-R. Park, E.-T. Hwang and K.-W. Park, *Mater. Lett.*, 2014, **124**, 231–234.
27 M. Hu, Y. Murakami, M. Ogura, S. Maruyama and T. Okubo, *J. Catal.*, 2004, **225**, 230–239.
28 T. Thurakitseree, C. Kramberger, P. Singjai and S. Maruyama, *Nanoscale*, 2017, **9**, 4002–4006.
29 T. Susi, Z. Zhu, G. Ruiz-Soria, R. Arenal, P. Ayala, A. G. Nasibulin, H. Lin, H. Jiang, O. Stephan, T. Pichler, A. Loiseau and E. I. Kauppinen, *Phys. Status Solidi B*, 2010, **247**, 2726–2729.
30 T. Susi, A. Kaskela, Z. Zhu, P. Ayala, R. Arenal, Y. Tian, P. Laiho, J. Mali, A. G. Nasibulin, H. Jiang, G. Lanzani, O. Stephan, K. Laasonen, T. Pichler, A. Loiseau and E. I. Kauppinen, *Chem. Mater.*, 2011, **23**, 2201–2208.
31 J. W. Jang, C. E. Lee, S. C. Lyu, T. J. Lee and C. J. Lee, *Appl. Phys. Lett.*, 2004, **84**, 2877–2879.
32 S. Maldonado, S. Morin and K. J. Stevenson, *Carbon*, 2006, **44**, 1429–1437.

33 L. G. Bulusheva, A. V. Okotrub, I. A. Kinloch, I. P. Asanov, A. G. Kurenya, A. G. Kudashov, X. Chen and H. Song, *Phys. Status Solidi B*, 2008, **245**, 1971–1974.

34 H. Liu, Y. Zhang, R. Li, X. Sun, S. Dsilets, H. Abou-Rachid, M. Jaidann and L.-S. Lussier, *Carbon*, 2010, **48**, 1498–1507.

35 C. Shan, W. Zhao, X. L. Lu, D. J. O'Brien, Y. Li, Z. Cao, A. L. Elias, R. Cruz-Silva, M. Terrones, B. Wei and J. Suhr, *Nano Lett.*, 2013, **13**, 5514–5520.

36 C. L. Pint, Z. Sun, S. Moghazy, Y.-Q. Xu, J. M. Tour and R. H. Hauge, *ACS Nano*, 2011, **5**, 6925–6934.

37 Y. T. Lee, N. S. Kim, S. Y. Bae, J. Park, S.-C. Yu, H. Ryu and H. J. Lee, *J. Phys. Chem. B*, 2003, **107**, 12958–12963.

38 F. Villalpando-Paez, A. Zamudio, A. Elias, H. Son, E. Barros, S. Chou, Y. Kim, H. Muramatsu, T. Hayashi, J. Kong, H. Terrones, G. Dresselhaus, M. Endo, M. Terrones and M. Dresselhaus, *Chem. Phys. Lett.*, 2006, **424**, 345–352.

39 Y.-S. Min, E. J. Bae, I. P. Asanov, U. J. Kim and W. Park, *Nanotechnology*, 2007, **18**, 285601.

40 S. Liu, Y. Zhang, Y. Lin, Z. Zhao and Q. Li, *Carbon*, 2014, **69**, 247–254.

Graphical Abstract

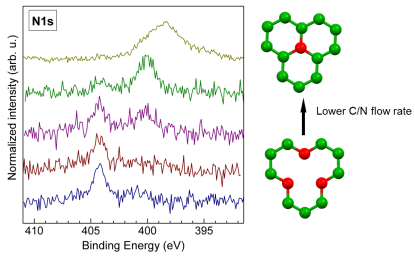

We demonstrate the modification of nitrogen configuration through CVD process. Lowering mixed carbon/nitrogen (C/N) feedstock flow rate could promote a predominance of pyridinic and graphitic nitrogen structures, while higher feedstock flow rates give rise to the formation of encapsulated N_2 molecules.